A peer-reviewed version of this preprint was published in PeerJ on 18 January 2017.

View the peer-reviewed version (peerj.com/articles/2887), which is the preferred citable publication unless you specifically need to cite this preprint.

Bialevich V, Sinha D, Shamayeva K, Guzanova A, Řeha D, Csefalvay E, Carey J, Weiserova M, Ettrich RH. 2017. The helical domain of the EcoR124I motor subunit participates in ATPase activity and dsDNA translocation. PeerJ 5:e2887 https://doi.org/10.7717/peerj.2887

PeerJ Preprints NOT PEER-REVIEWED

The helical domain of the EcoR124I motor subunit participates in ATPase activity and dsDNA translocation

Vitali Bialevich [1,2], **Dhiraj Sinha** [1,2], **Katsiaryna Shamayeva** [1], **Alena Guzanova** [3], **David Řeha** [1,2], **Eva Csefalvay** [1], **Jannette Carey** [1,4], **Marie Weiserova** [3], **Rüdiger H Ettrich** Corresp. [1,2,5]

[1] Center for Nanobiology and Structural Biology, Institute of Microbiology of the Academy of Sciences of the Czech Republic, Nove Hrady, Czech Republic
[2] Faculty of Sciences, University of South Bohemia, Nove Hrady, Czech Republic
[3] Institute of Microbiology, Academy of Sciences of the Czech Republic, Prague, Czech Republic
[4] Chemistry Department, Princeton University, Princeton, New Jersey, United States
[5] College of Medical Sciences, Nova Southeastern University, Fort Lauderdale, Florida, United States

Corresponding Author: Rüdiger H Ettrich
Email address: ettrich@nh.cas.cz

Type I restriction-modification enzymes are multisubunit, multifunctional molecular machines that recognize specific DNA target sequences, and their multisubunit organization underlies their multifunctionality. EcoR124I is the archetype of Type I restriction-modification family IC and is composed of three subunit types, HsdS, HsdM, and HsdR. DNA cleavage and ATP-dependent DNA translocation activities are housed in the distinct domains of the endonuclease/motor subunit HsdR. Because the multiple functions are integrated in this large subunit of 1038 residues, a large number of interdomain contacts might be expected. The crystal structure of EcoR124I HsdR reveals a surprisingly sparse number of contacts between helicase domain 2 and the C-terminal helical domain that is thought to be involved in assembly with HsdM. Only two potential hydrogen-bonding contacts are found in a very small contact region. In the present work, the relevance of these two potential hydrogen-bonding interactions for the multiple activities of EcoR124I is evaluated by analysing mutant enzymes using *in vivo* and *in vitro* experiments. Molecular dynamics simulations are employed to provide structural interpretation of the functional data. The results indicate that the helical C-terminal domain is involved in the DNA translocation, cleavage, and ATPase activities of HsdR, and a role in controlling those activities is suggested.

PeerJ Preprints NOT PEER-REVIEWED

The helical domain of the EcoR124I motor subunit participates in ATPase activity and dsDNA translocation

Vitali Bialevich [1,2,#], Dhiraj Sinhaj[1,2,#], Katsiaryna Shamayeva [1], Alena Guzanova [3], David Řeha [1,2], Eva Csefalvay [1], Jannette Carey [1,4], Marie Weiserova [3], Rüdiger H. Ettrich [1,2 5,]*

[1]Center for Nanobiology and Structural Biology, Institute of Microbiology Academy of Sciences of the Czech Republic, Zámek 136, 37333, Nové Hrady, Czech Republic

[2]Faculty of Sciences, University of South Bohemia in Ceske Budejovice, Zámek 136, CZ-373 33 Nové Hrady, Czech Republic

[3]Institute of Microbiology, Academy of Sciences of the Czech Republic, Vídeňská 1083, 142 20 Praha 4, Czech Republic

[4]Chemistry Department, Princeton University, Princeton, New Jersey 08544-1009, USA

[5]College of Medical Sciences, NOVA Southeastern University, Fort Lauderdale, Florida, 33314-7796, USA

[#] *these authors contributed equally and should be considered as first authors*

**corresponding author's email address: ettrich@nh.cas.cz*

Abstract

Type I restriction-modification enzymes are multisubunit, multifunctional molecular machines that recognize specific DNA target sequences, and their multisubunit organization underlies their multifunctionality. EcoR124I is the archetype of Type I restriction-modification family IC and is composed of three subunit types, HsdS, HsdM, and HsdR. DNA cleavage and ATP-dependent DNA translocation activities are housed in the distinct domains of the endonuclease/motor subunit HsdR. Because the multiple functions are integrated in this large subunit of 1038 residues, a large number of interdomain contacts might be expected. The crystal structure of EcoR124I HsdR reveals a surprisingly sparse number of contacts between helicase domain 2 and the C-terminal helical domain that is thought to be involved in assembly with HsdM. Only two potential hydrogen-bonding contacts are found in a very small contact region. In the present work, the relevance of these two potential hydrogen-bonding interactions for the multiple activities of EcoR124I is evaluated by analysing mutant enzymes using *in vivo* and *in vitro* experiments. Molecular dynamics simulations are employed to provide structural interpretation of the functional data. The results indicate that the helical C-terminal domain is involved in the DNA translocation, cleavage, and ATPase activities of HsdR, and a role in controlling those activities is suggested.

Introduction

Type I restriction-modification enzymes (RMs) are multisubunit, multifunctional molecular machines that recognize specific, typically asymmetric, DNA target sequences of ~13 to 14 bp (Murray, 2002). In sharp contrast to the straightforward mechanisms of the Type II RMs (Loenen et al., 2014), the multisubunit organization of Type I RM systems underlies their multifunctionality. Depending on the methylation status of adenine residues in the target sequence, three Type I subunits either act together as a typical methyltransferase, or recruit a pair of endonuclease motor subunits that initiate translocation of DNA through the enzyme and eventually cleave non-specifically at apparently random sites (Janscak et al., 1999). The protein complex remains bound at the target sequence while up to thousands of bp are pumped through the enzyme by tracking along the duplex helical pitch at rates of up to hundreds of bp per second (Bickle, Brack & Yuan, 1978; Studier & Bandyopadhyay, 1988; Szczelkun et al., 1996; Ellis et al., 1999; Seidel et al., 2004). Translocation is driven by RecA-helicase-like motor subunits that consume ~1 ATP per ~1 bp (Seidel et al., 2008) without separating the duplex strands (Stanley et al., 2006). The endonuclease activity of the motor subunits is unmasked under conditions that suggest a role for DNA topology in control of cleavage activity (Yuan, 1981; Janscak et al., 1999, Janscak & Bickle, 2000).

The X-ray crystal structure of the first Type I R-M motor subunit was solved in 2009 for EcoR124I from the *E. coli* plasmid pTrcR124 (Lapkouski et al, 2009). EcoR124I is the archetype of Type I R-M family IC and is composed of three distinct subunit types, HsdS, HsdM, and HsdR, which are encoded by the *hsd* (host specificity of DNA) genes. The fully assembled enzyme complex is a pentamer with $R_2M_2S_1$ stoichiometry (Janscak, Dryden & Firman, 1998; Mernagh et al., 1998). Small-angle neutron scattering experiments revealed the locations of HsdS and HsdM (Taylor et al., 2010), and electron microscopy and neutron and small-angle X-ray scattering (Kennaway et al., 2012) indicate that DNA binding triggers compaction of the $R_2M_2S_1$ enzyme from a conformation that has been described as more relaxed, loose, or open. The motor subunit HsdR is composed of four distinct structural and functional domains: an endonuclease domain at the N-terminus with characteristic motifs of the RecB nuclease superfamily (Obarska-Kosinska et al., 2008; Sisáková et al., 2008a; Sisáková et al., 2008b); a C-terminal α-helical domain proposed to contact methyltransferase (Davies et al., 1999); and two RecA-like helicase domains situated

between the endonuclease and C-terminal domains (Obarska-Kosinska et al., 2008; Lapkouski et al., 2009). Like other members of the SF2 translocase family, EcoR124I translocates on dsDNA (McClelland & Szczelkun, 2004; Firman & Szczelkun, 2000; Seidel et al, 2004) and lacks strand separation activity (Stanley et al., 2006). It has been proposed that helicase domain 1 contacts the 3'-5' dsDNA strand tightly during translocation, while helicase domain 2 is proposed to be responsible for DNA advancement through large and rapid conformational changes (Lewis et al., 2008).

Because both the translocase and endonuclease functions are part of the array of integrated structural domains in the large HsdR subunit of 1038 residues, a large number of interdomain contacts might be expected. However, the crystal structure of EcoR124I HsdR (Lapkouski et al., 2009) reveals a surprisingly sparse number of contacts particularly between the helical domain and helicase domain 2. The contact interface between the two domains is only 859 $Å^2$. Only a tiny fraction of it, 15 $Å^2$, is hydrophobic, and only two potential hydrogen-bonding contacts are found. One is centrally located between the two domains, a bifurcated contact in which the K527 sidechain atom Nζ is at a distance of 2.9 Å from the D796 carboxylate Oδ atom and 2.7 Å from the backbone carbonyl oxygen atom of N794. A second hydrogen bond is possible close to the short loop (K731-T734) that links the two domains, where the phenol O of Y736 is at a distance of 2.6 Å from the Oε2 atom of the E730 carboxylate (Fig. 1). These two hydrogen bonds constitute the only contacts detected at the domain interface. This finding led to a search for sequence similarities in the HsdR subunits of other Type I R-M enzymes that might support the significance of these contacts. The sequence alignment in figure 1C suggests that K527 may be part of a new motif that can be defined as (Q/D)KT that is also identified in the HsdR subunits of the EcoKI and EcoAI enzymes that typify Type I R-M families IA and IB. This proposal represents the first extension to all three Type I R-M families of a sequence alignment beyond the conserved DEAD-box motifs of the helicase active sites.

As helicase domain 2 is proposed to be the key player in DNA advancement, undergoing large conformational changes during the translocation cycle (Dürr et al., 2005), the question arises whether these two contacts to the helical domain have a role in the translocation cycle. If so, the helical domain itself could have a previously undescribed role in the translocation cycle beyond its presumed role in interacting with methyltransferase. In the present work, the relevance of these two potential hydrogen-bonding interactions for the translocation activity of EcoR124I is

evaluated by analysing mutant enzymes using *in vivo* and *in vitro* experiments. Molecular dynamics simulations are employed to provide structural interpretation of the functional data. The results suggest a role for the helical domain in DNA translocation.

Materials and Methods

Mutagenesis, expression and protein purification

Plasmid pTrcR124 (Janscak, Abadjieva & Firman, 1996) carrying the hsdR gene was used for site-directed mutagenesis. Oligonucleotide primers were used in the polymerase chain reaction (forward primer sequence is given, reverse primer is its complement; mutated codon underlined, changed nucleotides in bold): 5′-TTTCCGCCAG**GC**AACCCACCGTACC-3′ for K527A, 5′-GAGTTATACAGAG**GC**TATGGAAGGC-3′ for Y736A, and 5′-GCAAAACTAT**GC**TGAATTTGCCACG-3′ for D796A. The double mutant K527A_Y736A was obtained by introducing a second point mutation into the mutant plasmid Y736A.

The polymerase chain reaction was performed in 200 µl PCR tubes in an Eppendorf (Hamburg, Germany) mastercycler. The 20-µl reaction mixture contained 1.5 U Expand Long Range polymerase (Roche, Basel, Switzerland); 1X Expand Long Range Buffer with MgCl2; 100 ng of plasmid DNA pTrcR124; 0.3 µM each of the forward and reverse primers; 200 µM dNTPs; and 3 (v/v)% or 6 (v/v)% DMSO. PCR cycles were: 2 min at 96°C;30×(30s at 96°C,90s at 55°C,8min at 68°C); 7 min at 68 °C. DpnI (20 U) was used to degrade methylated parental plasmid. The reaction mixture was transformed into *E. coli* DH5α competent cells grown on LB-agar plates containing 100 µg/ml of ampicillin. Plasmid DNA was isolated using a Zyppy plasmid miniprep kit (Zymo Research, Irvine, CA, USA) and sequenced.

E. coli BL21(DE3) Gold competent cells were transformed with plasmid DNA containing the desired mutation. Overnight cultures were diluted 1:100 into 0.5 l of fresh LB medium in a 3-l flask supplemented to a final concentration of 100 µg ml^{-1} with ampicillin and incubated at 180 rpm at 37 °C until OD600 was about 0.5–0.6. IPTG was added to a final concentration of 1 mM and the culture was incubated for an additional 4 h at 37 °C and 30 °C for WT and mutant HsdR subunits, respectively. Harvested cells were washed in sodium chloride–Tris-EDTA buffer, pH 8.0. WT and mutant HsdR subunits were purified as described previously (Janscak, Abadjieva &

137 Firman, 1996). EcoR124I methyltransferase was expressed from pAC15M (Holubova et al., 2004)
138 and pJS491 (Patel et al., 1992) plasmids encoding HsdM and HsdS subunits, respectively, and
139 purified as described previously (Taylor et al., 1992). Purified methyltransferase and HsdR
140 subunits were mixed together in a 1:6 ratio to reconstitute the EcoR124I enzyme complex *in vitro*.
141
142 ***In vivo restriction activity assay***
143
144 *E.coli* strain JM109(DE3) (Yanisch-Perron, Vieira & Messing, 1985) served for complementation
145 analysis of restriction function *in vivo*. For negative complementation the pTrcR124 plasmid
146 expressing WT or mutants HsdR was transformed into *E. coli* JM109(DE3)[pKF650], a restricting
147 (r^+m^+) host containing all three *hsd* genes of EcoR124II. For positive complementation pTrcR124
148 was transformed into *E.coli* JM109(DE3)[pACMS] expressing only the EcoR124II
149 methyltransferase (r^-m^+) (Patel et al., 1992). Soft agar at 45 °C was mixed with 0.5 ml of each
150 fresh overnight culture, gently mixed, and immediately poured onto agar plates with appropriate
151 antibiotics. The virulent mutant of phage λ was used for testing of restriction phenotype (Jacob &
152 Wollman, 1954). Solidified soft agar was spotted with 30 µl each of tenfold serial dilutions of
153 λvir.0 phage lysate at 10^2 to 10^6 plaque-forming units/ml. The spots were dried at room
154 temperature and the plates incubated overnight at 37 °C (Colson et al., 1965). Phage buffer,
155 complex LB medium and *in vivo* restriction assays were as described (Hubácek, Holubová &
156 Weiserová, 1998; Sisáková et al., 2008b). The solid medium is LB with agar added at 1.5 (w/v)%.
157 Soft agar overlay is LB with agar added at 0.6 (w/v)%. Antibiotics were used at the following
158 concentrations: ampicillin; 100 mg ml^{-1}, chloramphenicol; 50 mg ml^{-1}. The efficiency of plating
159 was determined as the number of plaques on the tested strains compared to the number of plaques
160 on the non-restricting control strain *E. coli* JM109(DE3) (Yanisch-Perron, Vieira & Messing,
161 1985). Values in the range 0.0001–0.01 correspond to the restriction-competent (r+) phenotype,
162 those in the range 0.01–0.1 to the mixed-competence (r±) phenotype, and those in the range 0.1–
163 1 to the restriction-deficient (r−) phenotype.
164
165 ***In vitro cleavage activity assay***
166
167 Cleavage activity was assayed *in vitro* using supercoiled plasmid DNA substrate pRK (Taylor et

168 al., 1992) carrying a single recognition site for EcoR124I. Cleavage activity was assayed (Janscak
169 et al., 1996) at 37 °C in restriction buffer (50 mM Tris-HCl, pH 8.0, 1 mM DTT, 10 mM $MgCl_2$
170 and 50 mM NaCl) containing 15 nM of the circular pRK plasmid DNA, 15 nM methyltransferase
171 and 90 nM HsdR. After 1 min of pre-incubation the reaction was started by addition of ATP and
172 SAM to a final concentration 4 mM and 0.2 mM, respectively. The reaction was stopped by adding
173 0.25 vol of stop reagent (3 (w/v)% SDS; 0.15 M EDTA; 10 (w/v)% glycerol; 0.1 (w/v)%
174 bromophenol blue) and heating at 65 °C for 5 min. Samples were loaded into 1 (w/v)% agarose
175 gels in Tris-acetate-EDTA buffer and run at 5 V/cm for 130 min. Gels were stained with 2 µg/ml
176 ethidium bromide, destained in water and photographed under UV illumination. The relative
177 amounts of DNA were evaluated by densitometry using ImageJ software (Abramoff, Magalhaes
178 & Ram, 2004).
179
180 ***DNA Translocation assay – steady state analysis***
181
182 The method utilizes a fluorescently labeled triplex forming oligonucleotide (TFO) attached at a
183 specific distance from the EcoR124I binding site on plasmid DNA. Translocation by EcoR124I
184 leads to the dissociation of the triplex, which can be monitored by the change in fluorescence upon
185 displacement (Firman and Szczelkun, 2000; McClelland, Dryden & Szczelkun, 2005). Plasmid
186 pLKS5 carrying a DNA triplex binding site 1517 bp downstream of the EcoR124I recognition site
187 was used (L.K. Stanley and M.D. Szcelkun, 2006). Linear DNA for the triple-helix displacement
188 assay was generated by ApaI digestion of pLKS5 plasmid DNA followed by phenol/chloroform
189 extraction, chloroform extraction and isopropanol precipitation. The triplex was formed by
190 incubating 50 nM linear and 25 nM 5'-end Tetramethylrhodamine (TAMRA) labeled
191 oligonucleotide 5'-´TTTCTTCTTCTTTTCTTTTCTT-3´ (Eurofins MWG Operon) in buffer (10
192 mM MES pH 5.5, 12.5 mM $MgCl_2$) at 23°C overnight. Following overnight incubation, the triplex
193 was stored on ice, and then diluted 1/10 in reaction buffer (50 mM Tris-HCl, pH 8.0, 1 mM DTT,
194 10 mM MgCl2 and 50 mM NaCl) before use. 5 nM Triplex was pre-incubated with 40 nM MTase
195 and 120 nM wt or mutant HsdR at RT °C for 5 min. Following Simons & Szczelkun (2011) the
196 required concentration of the HsdR subunit for $R_2M_2S_1$ complex formation is twice that of the
197 DNA under the given conditions. A 120 nM concentration of HsdR (methyltransferase (M_2S_1) to
198 HsdR ratio 1:3) was enough to saturate both methyltransferase binding sites under experimental

199 conditions. Translocation reaction was initiated with 4 mM ATP and after 10 minutes triplex
200 displacement was measured. Steady state anisotropy for the bound (triplex) and free forms of
201 TAMRA labeled TFO was measured using a Tecan Safire 2 Multi-detection Microplate Reader.
202 Excitation and emission wavelengths used were: 544 and 576 nm, bandwidths were kept < 10nm.
203 Data are expressed as the means of three independent experiments.
204
205 ***ATPase activity assay in vitro***
206
207 ATPase activity was assayed using a radioactivity-based ATPase assay. In a first step cellulose
208 plates were prepared by marking positions for sample drops with a pencil: 1.5 cm from the bottom
209 of the plate and 1 cm in between dots. 50 ml of running buffer (0.4 M LiCl, 1 M Formic acid) or
210 water was carefully poured in the glass chamber, avoiding drops on the walls. At first each
211 cellulose plate was pre-run in running buffer and dried. Then the same steps were performed with
212 destilled water. Prepared plates can be stored at room temperature up to one week.
213 ATPase activity itself was assayed in NEB2 buffer containing 10 mM Tris-HCl, pH 7.9, 10 mM
214 $MgCl_2$, 50 mM NaCl, 1 mM DTT; 15 nM methyltransferase, 90 nM HsdR, and 6 molar excess (90
215 nM) of covalently closed circular DNA pRK containing single recognition site for EcoR124I to
216 prevent DNA cleavage. Excess of DNA concentration over enzyme was used (6:1 ratio) following
217 Janscak et al. (1996) and 6-folds excess in HsdR subunit concentration ensures efficient ATPase
218 activity as was described by Janscak, Dryden & Firman (1998). The HsdR subunit does not turn
219 over after cleavage of supercoiled DNA that might occur, nevertheless, ATPase activity is efficient
220 under tested conditions (Simons & Szczelkun, 2011). Reactions (40 µL) were started by addition
221 of ATP mixture containing 0.16 µCi (0.0013 mM) [γ^{32}P]-ATP to a final concentration of 2 mM
222 and incubated at 37 °C. Aliquots (4 µL) were taken at the indicated time points and stopped by
223 adding 1 (w/v)% SDS. The hydrolyzed $^{32}P_i$ was separated from [γ^{32}P]-ATP by cellulose TLC in
224 0.4 M $LiCl_2$, 1M formic acid (Randerath & Randerath, 1964) and the distribution of radioactivity
225 between $^{32}P_i$ and ATP was visualized using a Fujitsu 9000 scanner (Marini & Krejci, 2012).
226
227
228 ***Molecular dynamics simulations***
229

230 The WT crystal structure of the motor subunit HsdR from the restriction-modification system
231 EcoR124I (PDB entry 2W00) and a recent crystal structure of HsdR mutant Lys220Ala (PDB
232 entry 4BEC) were used for preparing the structural model for all simulations. Three missing
233 segments from the WT crystal structure (residues 142-147, 585-590, and 859-869) were built using
234 standard loop modeling in YASARA (Krieger, Koraimann & Vriend, 2002; Konagurthu et al.,
235 2006) and added to the WT crystal structure. The missing segment from residue 182 to 189 is
236 resolved in the Lys220Ala mutant crystal structure and thus was built into the WT structure by
237 adding the coordinates from the mutant to the above modeled structure, followed by steepest-
238 descent energy minimization. All classical MD simulations were performed using GROMACS
239 4.64 (Berendsen, van der Spoel & van Drunen, 1995; van der Spoel et al., 2005; Pronk et al., 2013)
240 with the AMBER99SB forcefield (Hornak et al., 2006). ATP was parameterized by applying the
241 standard RESP procedure using Antechamber (Wang et al., 2004), where charges for free MgATP
242 were derived from HF/6-31G* calculation in Gaussian03 (Frisch et al., 2003). Histidine was
243 assumed to be charged, with the ND and NE atoms protonated; arginine and lysine residues were
244 assumed to be protonated. Mutants were prepared *in silico* by replacing the respective side-chain
245 in YASARA followed by short minimization of 100 ps with freezing of all residues except those
246 close to each point mutation, to avoid any local crashes in the side-chain and then simulated for
247 100ns using classical molecular dynamics simulations and analyzed to evaluate possible
248 conformational changes. All systems were solvated in explicit TIP3P water (Jorgensen et al., 1983)
249 in a cubic box with a margin of 10 A and neutralized by adding sodium counterion. The particle-
250 mesh Ewald method (Darden et al., 1993) was applied to calculate long-range electrostatic
251 interactions with a cutoff distance of 10 Å and a Lennard-Jones 6-12 potential was used to evaluate
252 van der Waals interactions within 10 Å cutoff distance. The LINCS algorithm of fourth order
253 expansion was used to constrain bond lengths (Hess et al., 1997). After solvation and neutralization
254 each system was energy minimized for 10,000 step using steepest descent optimization method to
255 remove poor van der Waals contacts in the initial geometry. After minimization two stages of
256 equilibration were conducted. Firstly the system was equilibrated for 1 ns with position restraints
257 of 10000 KJ/mol on all heavy atoms. A constant temperature of 300 K was maintained using the
258 V-rescale algorithm (Bussi, Donadio &Parrinello, 2007) with a coupling time of 0.1 ps and
259 separate baths for the solute and the solvent. The pressure was kept constant at 1 bar using the
260 Parrinello-Rahman pressure coupling scheme (Parrinello & Rahman, 1981) with a time constant

of 2 ps. Initial velocities were generated randomly using a Maxwell-Boltzmann distribution corresponding to 300 K. Neighbor lists were updated every 10 fs using a group cut-off scheme. Finally the production run was performed for 100 ns without restraints at 300 K in the isothermal-isobaric ensemble.

Principal-component analysis (Amadei, Linnssen & Berendsen, 1993) was used using g_covar and g_anaeig tools in the GROMACS package to identify the global motions of the system using backbone atom only. The g_rms tool of the GROMACS package was used to calculate root mean square deviations (RMSD) during the trajectories taking the minimized crystal structure as reference. Root mean square fluctuations (RMSF) of the backbone of each residue were calculated by g_rmsf while atomic distances were measured by g_dist.

271 **Results**

272

273 **Restriction activity *in vivo***

274

275 The restriction activity of wild-type (WT) HsdR and all mutants was measured *in vivo* by
276 monitoring the ability of cells expressing WT HsdS-HsdM2 methyltransferase and WT or mutated
277 HsdR to restrict the growth of unmodified bacteriophage λvir.0. Positive and negative
278 complementation tests (Sisáková et al., 2008b), respectively, were used to distinguish between
279 defects in DNA cleavage and defects in the interaction of mutant HsdR subunits with
280 methyltransferase. Positive complementation uses a restriction-deficient (r-) host lacking WT
281 HsdR to test if a mutant HsdR subunit functions in DNA cleavage. Negative complementation uses
282 a restriction-competent (r+) host expressing WT HsdR to test if a mutant HsdR subunit that is
283 defective in DNA cleavage is competent for assembly with methyltransferase, allowing it to
284 compete with WT HsdR subunits and thus reduce their restriction activity. This effect is called a
285 trans-dominant effect. Wildtype HsdR complements restriction in the r^- host in the positive
286 complementation test (Table 1, r^- host), reducing λvir.0 infectivity as expected (value 0.001, within
287 the range 0.0001–0.01 expected for the restriction-proficient phenotype REF). All four mutants,
288 K527A, Y736A, K527A_Y736A, and D796A, fail to complement restriction in the r^- host (all
289 values within the range 0.1–1 expected for the restriction-deficient phenotype) and are therefore
290 restriction-deficient. In the negative complementation test the reduced restriction activity in the r^+
291 host (Table 1, r^+ host) indicates that all four mutant subunits are fully competent for assembly with
292 methyltransferase to form the endonuclease complex. The *in vivo* results thus support a role for
293 the helical domain in enzyme activity.

294

295 **DNA cleavage activity *in vitro***

296 DNA cleavage activity is tested *in vitro* on a covalently closed circular plasmid DNA containing
297 a single EcoR124I recognition site using the EcoR124I RM complex reconstituted with either WT
298 or mutant HsdR. DNA cleavage *in vitro* proceeds in two steps (Janscak et al., 1996). When
299 translocation is impeded the enzyme first cleaves one strand of the DNA duplex resulting in a
300 nicked DNA product, which is then linearized in a second step. Although cleavage is non-specific
301 and distant from the single recognition sequence, the resulting linearized DNAs are all of the same

302 length. For efficient DNA cleavage a 1:1 ratio of reconstituted EcoR124I R2M2S1 complex to
303 DNA and 6:1 ratio of HsdR subunits to methyltransferase (M_2S_1-complex) was used. An excess
304 of HsdR subunit over methyltransferase is required for successful formation of restriction-
305 proficient complexes with stoichiometry of $R_2M_2S_1$ because the second HsdR subunit binds to
306 methyltransferase with at least two orders of magnitude lower affinity than the first one (Janscak,
307 Dryden & Firman, 1998; Mernagh et al., 1998).
308 With reconstituted WT enzyme in 30 min of incubation, essentially all the circular substrate with
309 a single EcoR124I recognition site is cleaved on one or both strands, generating approximately
310 90% linear product and 10% nicked DNA ("open circle" on Fig 2.). Mutants K527A, Y736A, and
311 the double mutant K527A_Y736A are unable to cleave this circular DNA. Mutant D796A exhibits
312 measurable but significantly decreased cleavage activity compared to WT, with ~47 % of the DNA
313 remaining circular, ~35 % cleaved completely, and ~18 % nicked. To quantify the relative cleavage
314 rates of different mutant proteins, rate constants for the disappearance of supercoiled DNA were
315 estimated for WT and mutant D796A by fitting the data on Fig 2 with an exponential function.
316 The best-fit value of the rate constant λ for the reconstituted WT enzyme is 0.0238 s^{-1}, whereas the
317 rate constant λ for mutant D796A is approximately two thirds the WT value, 0.0154 s^{-1}. The
318 difference between WT and mutant values is in a similar range as found previously for other
319 mutants that display a restriction-deficient phenotype *in vivo* (Csefalvay, 2015). Thus the *in vivo*
320 results can be considered a more sensitive indication of enzyme activity than the *in vitro* results.
321
322 **Translocation activity *in vitro***
323
324 Translocation of duplex DNA by reconstituted WT and mutant enzymes was measured using a
325 triplex displacement assay. In this assay, a fluorescently-labeled oligonucleotide forms a DNA
326 triplex 1517 bp downstream of the recognition sequence and is displaced when this region of the
327 DNA passes through the enzyme during translocation (McClelland, Dryden & Szczelkun, 2005).
328 Complete displacement of the oligonucleotide by the enzyme results in a fluorescence signal
329 similar to that of the free oligonucleotide. At the DNA to methyltransferase ratio of 8:1 and
330 saturating concentration of HsdR subunits used in this assay, the single recognition site on the
331 circular DNA substrate is expected to be fully bound by the pentameric complex of EcoR124I with
332 stoichiometry$R_2M_2S_1$ (McClelland, Dryden & Szczelkun, 2005). In control experiments no triplex

333 displacement is observed in the absence of ATP or HsdR. Only the enzyme complex reconstituted
334 with WT HsdR results in fluorescence intensity similar to that of the free oligonucleotide. All four
335 mutant enzymes, K527A, Y736A, D796A, and K527A_Y736A, showed fluorescence intensities
336 similar to that of the initial DNA triplex with bound oligonucleotide (Fig. 3), indicating that these
337 enzymes do not displace the oligonucleotide and thus have lost the ability to translocate duplex
338 DNA. These results demonstrate that these point mutations in the helical domain affect
339 translocation.
340
341 **ATP hydrolysis *in vitro***
342
343 DNA-dependent ATPase activities were measured using the circular DNA substrate containing a
344 single EcoR124I recognition site after reconstitution of the purified WT and mutant HsdR subunits
345 with HsdS-HsdM$_2$ methyltransferase. Control assays omitting either DNA or methyltransferase
346 indicate negligible ATP hydrolysis. A relative ATPase activity of 100% was assigned to the
347 enzyme reconstituted with WT HsdR. The relative ATPase activity of reconstituted mutant
348 enzymes Y736A, K527A, and double mutant K527A_Y736A is ~25%, 16%, and 8%, respectively
349 (Fig. 4), indicating that these enzymes hydrolyze ATP very poorly *in vitro*, consistent with their
350 inability to translocate duplex DNA *in vitro*. However, reconstituted mutant enzyme D796A
351 exhibits a relative ATPase activity of ~88%, in apparent contradiction to its lack of translocation
352 activity in the triplex-displacement experiments. The finding that mutant D796A retains ATPase
353 activity but lacks translocation activity suggests that the correlation between these two activities
354 may be weaker than has been previously assumed (Abadjieva & Firman, 1996). Although ATPase
355 activity has been considered an indicator of translocation activity and is a necessary condition for
356 translocation, ATPase activity is only one component of translocation activity, and in this case it
357 is not sufficient for translocation. The decoupling of ATPase activity from translocation in the
358 D796A mutant may reflect structural or dynamic changes that cannot be further described at
359 present. Alternatively or additionally, the different temperatures for the translocation and ATPase
360 assays might be related to the inability to translocate efficiently despite ATPase activity. Under
361 the conditions tested here, although the D796A mutant was able to partially cleave the supercoiled
362 DNA substrate *in vitro*, the rate of DNA cleavage was insufficient for cells to survive phage
363 infection *in vivo*. Nevertheless, the inefficient ATP hydrolysis by three of the enzymes

364 reconstituted with mutant HsdR subunits indicates an unexpected role for the helical domain in
365 ATP hydrolysis.
366
367
368 **Molecular dynamics simulations**
369
370 The initial structure of the HsdR subunit used in the simulations presented here (Sinha et al., 2014)
371 is based on the published crystal structure (PDB id: 2W00, [Lapkouski et al, 2009]) with modeled
372 missing loops (residues 142-147, 585-590, and 859-869) built using standard loop modeling in
373 YASARA [Krieger et al., 2002; Konagurthu et al., 2006]. This structure has been shown previously
374 to be stable in MD simulations, and the resulting trajectories achieve equilibrium after 50ns of
375 simulation (Sinha et al., 2014) allowing simulations of 100 ns, which is sufficient to test the effect
376 of point mutations. Structures of single mutants K527A, D796A, and Y736A, and double mutant
377 K527A_Y736A were prepared by swapping each individual residue for the WT residue of the
378 starting structure in YASARA. The trajectories of WT and mutant HsdR subunits reveal that in all
379 cases the secondary structure is maintained throughout and the fold is preserved. In all simulations
380 the root mean square deviations (RMSD) from the starting structure reach a plateau of ~ 3 to 3.5
381 Å after 50 ns, comparable to equilibration times and RMSD values reported previously for the WT
382 HsdR system with modeled missing loops (Sinha et al., 2014) and acceptable for a system of this
383 size having multiple domains.
384
385 Global motions during the simulations were analyzed by principal components analysis (PCA).
386 Equilibrated trajectories for the final 20 ns of each individual WT or mutant simulation were
387 extracted and joined into one combined trajectory to allow calculation of the first eigenvector that
388 identifies the motion with the largest change (Fig. 5). The global collective motion described by
389 the first eigenvector for mutants K527A, Y736, and K527A_Y736A is a partial opening of the
390 cleft between helicase domains 1 and 2, due mainly to movement of helicase domain 2. Mutant
391 D796A and WT HsdR maintain the starting conformation of the WT subunit, in which the cleft
392 remains closed. Projections along the first eigenvector were analyzed to quantify these structural
393 changes (Fig. 6). These projections describe the extent to which themotion described by the first
394 eigenvector is present in the simulation of each protein. WT HsdR shows no major change along

395 the first eigenvector and its projection value oscillates around zero, as expected because the initial
396 WT structure represents an energy-minimized and equilibrated structure. Like WT HsdR, mutant
397 D796A shows no change along the first eigenvector and its projection oscillates around zero,
398 indicating no opening of the cleft between the two helicase subunits. In contrast, K527A, Y736A,
399 and double mutant K527A_Y736A move ~10 +/- 2 Å along the first eigenvector, indicating
400 considerable movement of helicase domain 2 away from helicase domain 1 to open the cleft
401 compared with the initial crystal structure.
402 These global structural changes of helicase domain 2 during the simulations are also reflected in
403 the rmsd values calculated for C-alpha atoms by superimposing the last snapshot of each simulated
404 structure on the WT crystal structure. During 100ns of WT MD simulation helicase domain 2 stays
405 in a position almost identical to that in the crystal, with a maximum rmsd of ~ 0.2 Å. Significant
406 structural changes occur during the simulations of mutants Y736A, K527A, and double mutant
407 K527A_Y736A, with maximum rmsd values of ~ 4.1 Å, ~ 3.8 Å, and ~ 2.8 Å, respectively. Mutant
408 D796A shows a maximum rmsd of ~ 0.6 Å, indicating only a minor conformational change similar
409 to that observed in WT. The interdomain distances between centers of mass of the two helicase
410 domains confirm the helicase cleft opening in mutants K527A, Y736A, and K527A_Y736A,
411 whereas in mutant D796A the two domains are somewhat closer to each other than in WT (Table
412 2).
413 These results suggest that loss of the limited interdomain contacts between the helical
414 domain and helicase domain 2 leads to substantial structural changes in mutants K527A, Y736A,
415 and double mutant K527A_Y736A, characterized by opening of the cleft between the two helicase
416 domains located ~25 Å away from the site of these mutations. Such a long-range effect is further
417 indication of an integral role for the helical domain in HsdR function. In contrast, in WT and
418 mutant D796A HsdR, helicase domain 2 largely maintains the conformation observed in the WT
419 crystal structure. This result suggests that in the D796A mutant K527 may be able to maintain at
420 least partial contact with the helical domain even though D796 is no longer available as a partner.
421 To further evaluate this possibility a more subtle interaction analysis of the simulation results was
422 carried out.
423 The persistence of the interdomain contacts observed in the crystal structure was analyzed
424 in the equilibrated part of each simulation. Although neither H atoms nor hydrogen bonds are
425 detectable in crystal structures, H atoms are included in the calculations based on predicted

426 covalent geometries (Berendsen, van der Spoel & van Drunen, 1995). Hydrogen bonds are
427 observed between the K527 amino group and two acceptors, the backbone carbonyl O atom of
428 N794 and the carboxylate Oδ atom of D796, and between the hydroxyl group of Y736 and
429 carboxylate Oε atom of E730 in the short loop linking the two domains. Panel A in Figure 7 reveals
430 that during simulation of WT HsdR the hydrogen bond between the K527 amino group and the
431 backbone carbonyl O atom of N794 is lost completely after 20 ns, whereas the hydrogen bond
432 between the amino group of K527 and the carboxylate Oδ atom of D796 is maintained. The
433 hydrogen bond between the Y736 hydroxyl and the E730 carboxylate is maintained throughout
434 the simulation in WT (Fig. 7, panel B). In mutant D796A the hydrogen bond between the K527
435 amino group and the D796 carboxylate is no longer possible. The contact between the K527 amino
436 group and the N794 backbone carbonyl O atom is maintained after the initial equilibration time
437 (Fig 7, panel C), as is the interaction between the Y736 hydroxyl and the E730 carboxylate (Fig.
438 7, panel D). The resulting conformation of mutant D796A is thus very similar to WT throughout
439 the simulation, showing no large-scale domain movement although its interactions at the helical-
440 helicase interface differ locally.
441 Although mutant K527A is unable to hydrogen bond with either N794 or D796 as a result of the
442 point mutation, the Y736-E730 contact close to the short loop linking the two domains persists
443 throughout the simulation. Mutant Y736A does not form the hydrogen bond close to the short loop
444 linking the two domains, and the interaction between the K527 amino group and the carboxylate
445 Oδ atom of D796 is also lost completely during equilibration. Only a contact between the K527
446 amino group and the backbone carbonyl O atom of N794 is persistent. Finally, analysis of H-bond
447 numbers at the interface between helicase domains 1 and 2 during the simulations suggests a
448 correlation with helicase cleft opening (Table 2). Thus, double mutant K527A_Y736A with the
449 largest interdomain distance displays only up to 9 interdomain H-bonds compared to ~13 in WT
450 HsdR, whereas closure of the cleft in mutant D796A is correlated with up to 18 H-bonds at the
451 interdomain interface.
452
453 **Discussion**
454
455 The structurally characterized homologs of HsdR are the RecA-like SF2 helicases for its
456 translocation activity and the Type II restriction endonucleases for its endonuclease activity. Both

457 these homologs carry out their enzyme activity as isolated proteins with no additional functional
458 domains nor assembly with other subunits required. The HsdR subunit in contrast is a single
459 polypeptide chain that represents a symbiotic fusion of two RecA-like helicase domains with folds
460 characteristic of SF2 helicases, an endonuclease domain characteristic of the Type II enzymes, and
461 an auxiliary C-terminal helical domain. Based on the results presented here, the role of the helical
462 domain can now be said to include participation in all the individual activities of the HsdR motor
463 subunit: DNA cleavage, DNA translocation, and ATP hydrolysis.

464 Because the observed interdomain interactions contribute to enzymatic function as
465 described in this work, they may be conserved in other Type1 restriction-modification systems in
466 which single HsdR subunits have multiple functions. Sequence alignment suggests that the main
467 interaction partner identified here in helicase domain 2, K527, is conserved throughout Type I R-
468 M families IA, IB, IC as part of a proposed new (Q/D)KT motif (Figure 1C). A similar three-
469 dimensional arrangement and function can be suggested for this region of these other Type I R-M
470 systems. Other related translocases from the SF2 superfamily such as Rad54 display low sequence
471 identity in this region, suggesting that the (Q/D)KT motif may be conserved specifically in the
472 Type I R-M systems, which require interdomain contact between helicase domain 2 and the helical
473 domain to integrate the functions of the domains.

474 The present work demonstrates a previously unsuspected role for the helical C-terminal
475 domain of the HsdR motor subunit in DNA translocation, cleavage, and ATPase activities. This
476 domain has been assumed to be involved in assembly with the HsdS/M methylase (Dryden et al.,
477 2001; Obarska-Kosinska et al., 2008). A role involving all three of the subunit's activities
478 implicates the C-terminal domain in controlling enzymatic function. Thus a controlling function
479 resides at a nexus of intersubunit communication.

480

481 **Acknowledgements**

482 The authors wish to thank Dr. Ladislav Cséfalvay for his assistance with ATPase activity assays.

483 **References**

484 Abadjieva A, Firman K 1996. The type I restriction endonuclease R.EcoR124I: over-production
485 and biochemical properties. *J Mol Biol* 257(5): 977–991.

486 Abramoff MD, Magalhaes PJ, Ram SJ. 2004. Image processing with ImageJ. *Biophotonics*
487 *international* 11:36–42.

488 Amadei A, Linnssen AB, Berendsen HJ. 1993. Essential dynamics of proteins. *Proteins* 17:412–
489 25.

490 Berendsen HJC, van der Spoel D, van Drunen R. 1995. GROMACS: a message-passing parallel
491 molecular dynamics implementation. *Computer Physics Communications* 91:43–56. DOI:
492 10.1016/0010-4655(95)00042-E.

493 Bickle TA, Brack C, Yuan R. 1978. ATP-induced conformational changes in the restriction
494 endonuclease from Escherichia coli K-12. *Proceedings of the National Academy of Sciences*
495 *USA* 75:3099–3103.

496 Bussi G, Donadio D, Parrinello M. 2007. Canonical sampling through velocity rescaling. *Journal*
497 *of Chemical Physics* 126:014101.

498 Colson C, Glover SW, Symons N, Stanley KA. 1965. The location of the genes for host-
499 controlled modification and restriction in *Escherichia coli* K-12. *Genetics* 52:1043–1050.

500 Csefalvay E, Lapkouski M, Guzanova A, Csefalvay L, Baikova T, Shevelev I, Bialevich V,
501 Shamayeva K, Janscak P, Kuta Smatanova I, Panjikar S, Carey J, Weiserova M, Ettrich R. 2015.
502 Functional coupling of duplex translocation to DNA cleavage in a Type I restriction enzyme.
503 *PLoS One* 10:e0128700. DOI: 10.1371/journal.pone.0128700.

504 Darden T, York D, Pedersen L, Ewald P. 1993. An N·log(N) method for Ewald sums in large
505 systems. *Journal of Chemical Physics* 98:10089–10092.

506 Davies GP, Martin I, Sturrock SS, Cronshaw A, Murray NE, Dryden DT. 1999. On the structure
507 and operation of type I DNA restriction enzymes. *Journal of Molecular Biology* 290:565-579.
508 Dryden DTF, Murray, NE & Rao DN. 2001. Nucleoside triphosphate-dependent restriction

509 enzymes. *Nucleic Acids Res*. 29: 3728–3741.

510 Dürr H, Körner C, Müller M, Hickmann V, Hopfner KP. 2005. X-ray structures of the
511 Sulfolobus solfataricus SWI2/SNF2 ATPase core and its complex with DNA. *Cell* 121: 363–373.

512 Ellis DJ, Dryden DTF, Berge T, Edwardson JM, Henderson RM. 1999. Direct observation of
513 DNA translocation and cleavage by the EcoKI endonuclease using atomic force microscopy.
514 *Nature Structural & Molecular Biology* 6:15–17.

515 Firman K, Szczelkun MD 2000. Measuring motion on DNA by the type I restriction
516 endonuclease EcoR1241 using triplex displacement. *EMBO Journal*. 19:2094-2102. DOI:
517 10.1093/emboj/19.9.2094.

518 Frisch MJ, Trucks GW, Schlegel HB, Scuseria GE, Robb MA, Cheeseman JR, Montgomery
519 JrJA, Vreven T, Kudin KN, Burant JC, Millam JM, Iyengar SS, Tomasi J, Barone V, Mennucci
520 B, Cossi M, Scalmani G, Rega N, Petersson GA, Nakatsuji H, Hada M, Ehara M, Toyota K,
521 Fukuda R, Hasegawa J, Ishida M, Nakajima T, Honda Y, Kitao O, Nakai H, Klene M, Li X,
522 Knox JE, Hratchian HP, Cross JB, Bakken V, Adamo C, Jaramillo J, Gomperts R, Stratmann
523 RE, Yazyev O, Austin AJ, Cammi R, Pomelli C, Ochterski JW, Ayala PY, Morokuma K, Voth
524 GA, Salvador P, Dannenberg JJ, Zakrzewski VG, Dapprich S, Daniels AD, Strain MC, Farkas O,
525 Malick DK, Rabuck AD, Raghavachari K, Foresman JB, Ortiz JV, Cui Q, Baboul AG, Clifford
526 S, Cioslowski J, Stefanov BB, Liu G, Liashenko A, Piskorz P, Komaromi I, Martin RL, Fox DJ,
527 Keith T, Al-Laham MA, Peng CY, Nanayakkara A, Challacombe M, Gill PMW, Johnson B,
528 Chen W, Wong MW, Gonzalez C, and Pople JA, 2004. GAUSSIAN 03 (revision C.02).
529 Gaussian, Inc., Wallingford.

530 Hess B, Bekker H, Berendsen HJC, Fraaije JGEM. 1997. LINCS: a linear constraint solver for
531 molecular simulations. *Journal of Computational Chemistry* 18:1463–1472.

532 Holubová I, Vejsadová S, Firman K, Weiserová M. 2004. Cellular localization of type I
533 restriction-modification enzymes is family dependent. *Biochemical and Biophysical Research*
534 *Communications* 319:375–380.

535 Hornak V, Abel R, Okur A, Strockbine B, Roitberg A, Simmerling C. 2006. Comparison of
536 multiple AMBER force fields and development of improved protein backbone parameters.
537 *Proteins* 65:712–725.

538 Hubácek J, Holubová I, Weiserová M. 1998. The effect of recA mutation on the expression of
539 EcoKI and EcoR124I hsd genes cloned in a multicopy plasmid. *Folia Microbiologica* 43:353-
540 359.

541 Jacob F, Wollman EL. 1954. Etude génétique d'un bactériophage tempéré d'Escherichia coli. III.
542 Effet du rayonnement ultraviolet sur la recombinaison génétique. *Annales de l'Institut Pasteur*
543 87:653-673.

544

545 Janscak P, Abadjieva A, Firman K. 1996. The type I restriction endonuclease R.EcoR124I: over-
546 production and biochemical properties *Journal of Molecular Biology* 257:977–991.

547 Janscak P, Bickle TA. 2000. DNA supercoiling during ATP-dependent DNA translocation by the
548 type I restriction enzyme EcoAI. *Journal of Molecular Biology* 295:1089-1099.

549 Janscak P, Dryden DTF, Firman K. 1998. Analysis of the subunit assembly of the type IC
550 restriction–modification enzyme EcoR124I. *Nucleic Acids Research* 26:4439–4445.

551 Janscak P, MacWilliams MP, Sandmeier U, Nagaraja V, Bickle TA. 1999. DNA translocation
552 blockage, a general mechanism of cleavage site selection by type I restriction enzymes. *EMBO*
553 *Journal* 18:2638-2647.

554 Jorgensen WL, Chandrasekhar J, Madura JD, Impey RW, Klein ML. 1983. Comparison of
555 simple potential functions for simulating liquid water. *Journal of Chemical Physics* 79:926.

556 Kennaway CK, Taylor JE, Song CF, Potrzebowski W, Nicholson W, White JH, Swiderska A,
557 Obarska-Kosinska A, Callow P, Cooper LP, Roberts GA, Artero J-B, Bujnicki JM, Trinick J,
558 Kneale GG & Dryden DTF. 2012. Structure and operation of the DNA-translocating type I DNA
559 restriction enzymes. *Genes & Development* 26(1):92-104. DOI: 10.1101/gad.179085.111.

560 Konagurthu AS, Whisstock JC, Stuckey PJ, Lesk AM. 2006. MUSTANG: a multiple structural
561 alignment algorithm. *Proteins* 64: 559–574.

562 Krieger E, Koraimann G, Vriend G. 2002. Increasing the precision of comparative models with
563 YASARA NOVA; a self-parameterizing force field. *Proteins* 47:393–402.

564 Lapkouski M, Panjikar S, Janscak P, Smatanova IK, Carey J, Ettrich R, Csefalvay E. 2009.
565 Structure of the motor subunit of type I restriction-modification complex EcoR124I. *Nature*
566 *Structural & Molecular Biology* 16:94–95. DOI:10.1038/nsmb.1523.

567 Lewis R, Dürr H, Hopfner KP, Michaelis J. 2008. Conformational changes of a Swi2/Snf2
568 ATPase during its mechano-chemical cycle. *Nucleic Acids Research* 36:1881-1890. DOI:
569 10.1093/nar/gkn040.

570 Loenen WAM, Dryden DTF, Raleigh EA, Wilson GG, Murray NE. 2014. Highlights of the DNA
571 cutters: a short history of the restriction enzymes. *Nucleic Acids Research*. 42:3-19. DOI:
572 10.1093/nar/gkt990.

573 Marini V, Krejci L. 2012. Unwinding of synthetic replication and recombination substrates by
574 Srs2. *DNA Repair* 11:789–798. DOI: 10.1016/j.dnarep.2012.05.007.

575 McClelland SE, Dryden DT, Szczelkun MD. 2005. Continuous assays for DNA translocation
576 using fluorescent triplex dissociation: application to type I restriction endonucleases. *Journal of*
577 *Molecular Biology* 348:895–915.

578 McClelland SE, Szczelkun M.D. 2004. The Type I and III restriction endonucleases: structural
579 elements in molecular motors that process DNA. In: Pingound A, ed. *Nucleic Acids and*
580 *Molecular Biology – Restriction Endonucleases*. Berlin, Germany, Springer Verlag, Vol. 14, 111
581 – 135.

582 Mernagh DR, Janscak P, Firman K & Kneale GG. 1998. Protei-protein and protein-DNA
583 interactions in the type I restriction endonuclease R.EcoR124I. *Biological Chemistry* 379, 497-
584 503.

585 Murray NE. 2002. Immigration control of DNA in bacteria: self versus non-self. *Microbiology*
586 148:3–20.

587 Obarska-Kosinska A, Taylor JE, Callow P, Orlowski J, Bujnicki JM, Kneale GG. 2008. HsdR
588 subunit of the type I restriction-modification enzyme EcoR124I: biophysical characterisation and
589 structural modelling. *Journal of Molecular Biology* 376:438-52. DOI:
590 10.1016/j.jmb.2007.11.024.

591 Parrinello M, Rahman A. 1981. Polymorphic transitions in single crystals: a new molecular
592 dynamics method. *Journal of Applied Physics* 52:7182.

593 Patel J, Taylor I, Dutta CF, Kneale G, Firman K. 1992. High-level expression of the cloned
594 genes encoding the subunits of and the intact DNA methyltransferase, M.EcoR124. *Gene*,
595 112:21–27.

596 Pronk S, Pall S, Schulz R, Larsson P, Bjelkmar P, Apostolov R, Shirts MR, Smith JC, Kasson
597 PM, van der Spoel D, Hess B, Lindahl E. 2013. GROMACS 4.5: a high-throughput and highly
598 parallel open source molecular simulation toolkit. *Bioinformatics* 29:845–854. DOI:
599 10.1093/bioinformatics/btt055.

600 Randerath K, Randerath E. 1964. Ion-exchange chromatography of nucleotides on poly-
601 (ethyleneimine)-celluslose thin layers. *Journal of Chromatography* 16:111–125.

602 Seidel R, van Noort J, van der Scheer C, Bloom JG, Dekker NH, Dutta CF, Blundell A,
603 Robinson T, Firman K, Dekker C. 2004. Real-time observation of DNA translocation by the type
604 I restriction modification enzyme EcoR124I. *Nature Structural & Molecular Biology* 11:838–
605 843.

606 Seidel R, Bloom JGP, Dekker C, Szczelkun MD. 2008. Motor step size and ATP coupling
607 efficiency of the dsDNA translocase EcoR124I. *EMBO Journal* 27:1388–1398. DOI:
608 10.1038/emboj.2008.69.

609 Simons M & Szczelkun MD. 2011. Recycling of protein subunits during DNA translocation and
610 cleavage by Type I restriction-modification enzymes. *Nucleic Acids Research*, 39, 7656–7666.

611 DOI: 10.1093/nar/gkr479.

612 Sinha D, Shamayeva K, Ramasubramani V, Řeha D, Bialevich V, Khabiri M, Guzanová A,
613 Milbar N, Weiserová M, Csefalvay E, Carey J, Ettrich R. 2014. Interdomain communication in
614 the endonuclease/motor subunit of Type I restrictionmodification enzyme EcoR124I. *Journal of*
615 *Molecular Modeling* 20:2334. DOI: 10.1007/s00894-014-2334-1.

616 Sisáková E, Stanley LK, Weiserová M, Szczelkun MD. 2008a. A RecB-family nuclease motif in
617 the Type I restriction endonuclease EcoR124I. *Nucleic Acids Research* 36:3939-3949. DOI:
618 10.1093/nar/gkn333.

619 Sisáková E, Weiserová M, Dekker C, Seidel R, Szczelkun MD. 2008b. The interrelationship of
620 helicase and nuclease domains during DNA translocation by the molecular motor EcoR124I.
621 *Journal of Molecular Biology* 384:1273-86. DOI: 10.1016/j.jmb.2008.10.017.

622 Stanley LK, Seidel R, van der Scheer C, Dekker NH, Szczelkun MD, Dekker C. 2006. When a
623 helicase is not a helicase: dsDNA tracking by the motor protein EcoR124I. *EMBO Journal*
624 25:2230-2239.

625 Studier FW, Bandyopadhyay PK. 1988. Model for how type I restriction enzymes select
626 cleavage sites in DNA. *Proceedings of the National Academy of Sciences USA* 85:4677–4681.

627 Szczelkun MD, Dillingham MS, Janscak P, Firman K, Halford SE. 1996. Repercussions of DNA
628 tracking by the type IC restriction endonuclease EcoR124I on linear, circular and catenated
629 substrates. *EMBO Journal* 15:6335–6347.

630 Taylor I, Patel J, Firman K, Kneale G. 1992. Purification and biochemical characterisation of the
631 EcoR124 type I modification methylase. *Nucleic Acids Research* 20:179–186.

632 Taylor JE, Callow P, Swiderska A, Kneale GG. 2010. Structural and functional analysis of the
633 engineered type I DNA methyltransferase EcoR124I(NT). *Journal of Molecular Biology* 398(3),
634 391-9. DOI: 10.1016/j.jmb.2010.03.008.

635 Van Der Spoel D, Lindahl E, Hess B, Groenhof G, Mark AE, Berendsen HJ. 2005. GROMACS:
636 fast, flexible, and free. *Journal of Computational Chemistry* 26:1701–1718.

637 Wang J, Wolf RM, Caldwell JW, Kollman PA, Case DA. 2004. Development and testing of a
638 general AMBER force field. *Journal of Computational Chemistry* 25:1157–1174.

639 Yanisch-Perron C, Vieira J, Messing J. 1985. Improved M13 phage cloning vectors and host
640 strains: nucleotide sequences of the M13mp18 and pUC19 vectors. *Gene* 33:103–119.

641 Yuan R. 1981. Structure and Mechanism of Multifunctional Restriction Endonucleases. *Annual*
642 *Review of Biochemistry* 50:285-315. DOI: 10.1146/annurev.bi.50.070181.001441.
643
644
645
646
647
648

PeerJ Preprints NOT PEER-REVIEWED

Table 1 (on next page)

Table 1. Effect of mutations on the restriction phenotype of EcoR124I

PeerJ Preprints NOT PEER-REVIEWED

1

2

	restriction[a]		Ability of cleavage	Ability of assembly
HsdR	**r− host [b]**	**r+ host[c]**		
WT	0.0012±0.0005[SD]	0.0011±0.0004	Yes	Yes
K527A	0.4388±0.3009	0.1092±0.0857	No	Yes
Y736A	0.3197±0.2147	0.2307±0.0694	No	Yes
K527A+Y736A	0.4230±0.1953	0.1619±0.0666	No	Yes
D796A	0.3962±0.0885	0.1965±0.1335	No	Yes

3

4 [a] restriction activity was determined as the efficiency of plating of λvir.0 on tested strains
5 relative to the efficiency of plating of λvir.0 on *E. coli* JM109(DE3) indicator (nonrestricting)
6 strain.
7 [b] The positive complementation was tested in r− host *E. coli* JM109(DE3)[pACMS] (r−m+).
8 [c] negative complementation (transdominant effect) in r+ host *E. coli* JM109(DE3)[pKF650]
9 (r+m+).
10 SD - standard deviation
11
12

PeerJ Preprints NOT PEER-REVIEWED

Table 2 (on next page)

Table 2. Interdomain distances and H-bonding between helicase I and helicase II domains

PeerJ Preprints NOT PEER-REVIEWED

1

2

	Avg. Inter-domain distance(Å)	Avg. Number of Interactions (H-bond)
WT	29.30 +/- .14	13 +/- 1.40
K527A	29.77 +/- .18	10 +/- 1.05
Y736A	29.90 +/- .17	09 +/- 1.17
K527A_Y736A	30.30+/- .21	09 +/- 1.05
D796A	29.01 +/- .13	17 +/- 2.11

3

4

5

PeerJ Preprints | https://doi.org/10.7287/peerj.preprints.2680v1 | CC BY 4.0 Open Access | rec: 2 Jan 2017, publ: 2 Jan 2017

PeerJ Preprints NOT PEER-REVIEWED

6

7

Figure 1

Figure 1. Interdomain interactions at the helical-helicase 2 domain interface in the HsdR subunit of EcoR124I restriction-modification complex.

A. The structure of HsdR consisting of four domains: the endonuclease domain is in yellow, the helicase 1 and the helicase 2 domains are depicted in cyan and magenta, respectively. The C-terminal helical domain is shown in green. ATP is represented in elemental colors as a skeletal model with cyan carbons, and magnesium is indicated by a yellow sphere. The modelled parts of the structure (not resolved in the crystal structure) are in orange and the modeled 180s loop comprising residues 182–189 that is close to the catalytic site on the endonuclease domain is in red just below ATP (coordinates borrowed from K220A mutant HsdR crystal structure ((PDB id: 4BEC, Csefalvay *et al.*, 2015)). The short linker between helicase 2 domain and the C-terminal helical domain is in grey at the lower right corner of the black rectangle **B.** Enlargement of the region enclosed by the black rectangle in panel A, showing residues involved in interactions at the interface between the helical domain and helicase domain 2. Side chains are shown as skeletal models in atomic colors with carbon atoms colored according to their subunit shown in panel A. Hydrogen bonding interactions discussed in the text are indicated with black dotted lines. **C.** Alignment of the interface region sequence of EcoR124I from family IC of with sequences from HsdR of the archetypical members of the other two type I R-M families, EcoKI from family IA and EcoAI from family IB. Secondary structures of Eco124I HsdR from the crystal strutcure (pdb code: 2w00) are shown on top. Colors and symbols below the sequences indicate residue similarity: '*' fully conserved residues; ':' highly similar residues; and '.' somewhat similar residues.

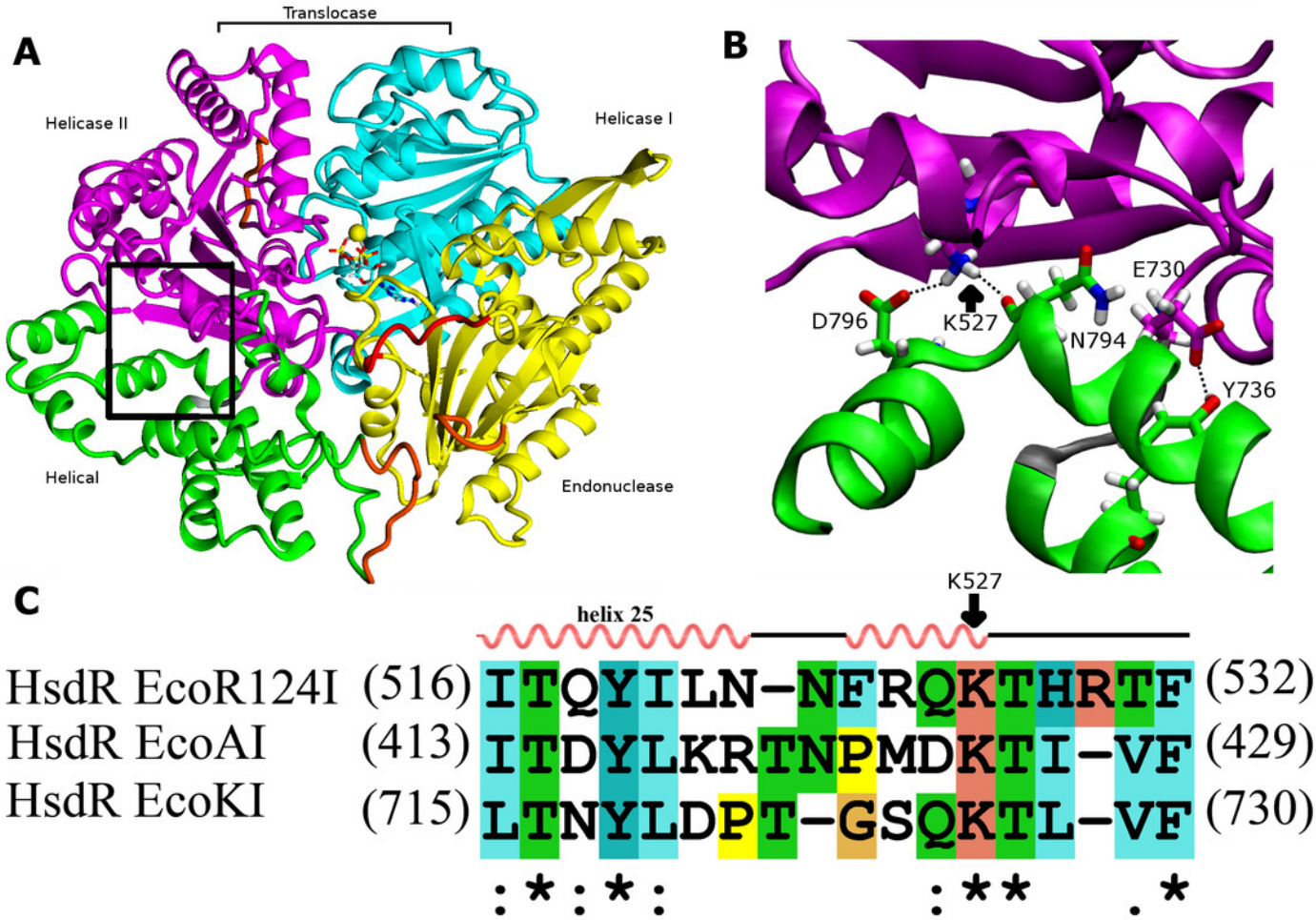
A
Translocase
Helicase II
Helicase I
Helical
Endonuclease
B
D796
K527
E730
N794
Y736
C
helix 25
K527
HsdR EcoR124I (516) ITQYILN-NFRQKTHRTF (532)
HsdR EcoAI (413) ITDYLKRTNPMDKTI-VF (429)
HsdR EcoKI (715) LTNYLDPT-GSQKTL-VF (730)
:*:*: :** .*

Figure 2

Figure 2. Cleavage of supercoiled substrate.

A. Supercoiled DNA substrate plasmid pRK carrying single EcoR124I recognition site is cleaved by EcoR124I R-M complex *in vitro*. EcoR124I was reconstituted from HsdS1HsdM2 methyltransferase and A) WT HsdR or mutant HsdRs B) K527A, C) Y736A, D) K527A_Y736A and E) D796A. Aliquots were quenched at the time points indicated in seconds and resolved on agarose gels stained with ethidium bromide. On panel A open circle and linear products are denoted as OC and L, respectively, and supercoiled substrate as SC; control (plasmid pRK linearized by HindIII restriction enzyme) is denoted as C; DNA molecular weight marker (M) with marked band size in kb on panel A. **B.** Quantification. DNA species were quantified using ImageJ software [Abramoff, Magalhaes & Ram, 2004]. Gels were scanned under UV illumination, and the image converted to grey scale and then inverted. The band density in the lane at time zero (before initiation of the reaction with ATP) is taken as 100 % of supercoiled substrate. The three indicated DNA species OC, open circular product (▲); L, linear product (●); SC, supercoiled substrate (■) were quantified individually from densities of bands in the gels on the left panels. Error bars represent standard deviations calculated from at least three independent experiments for each enzyme. Rates for the decrease of supercoiled DNA substrate were derived by fitting an exponential decay function to the data in SigmaPlot (solid lines); dashed lines connect the points only to guide the eye and do not represent fits to the data.

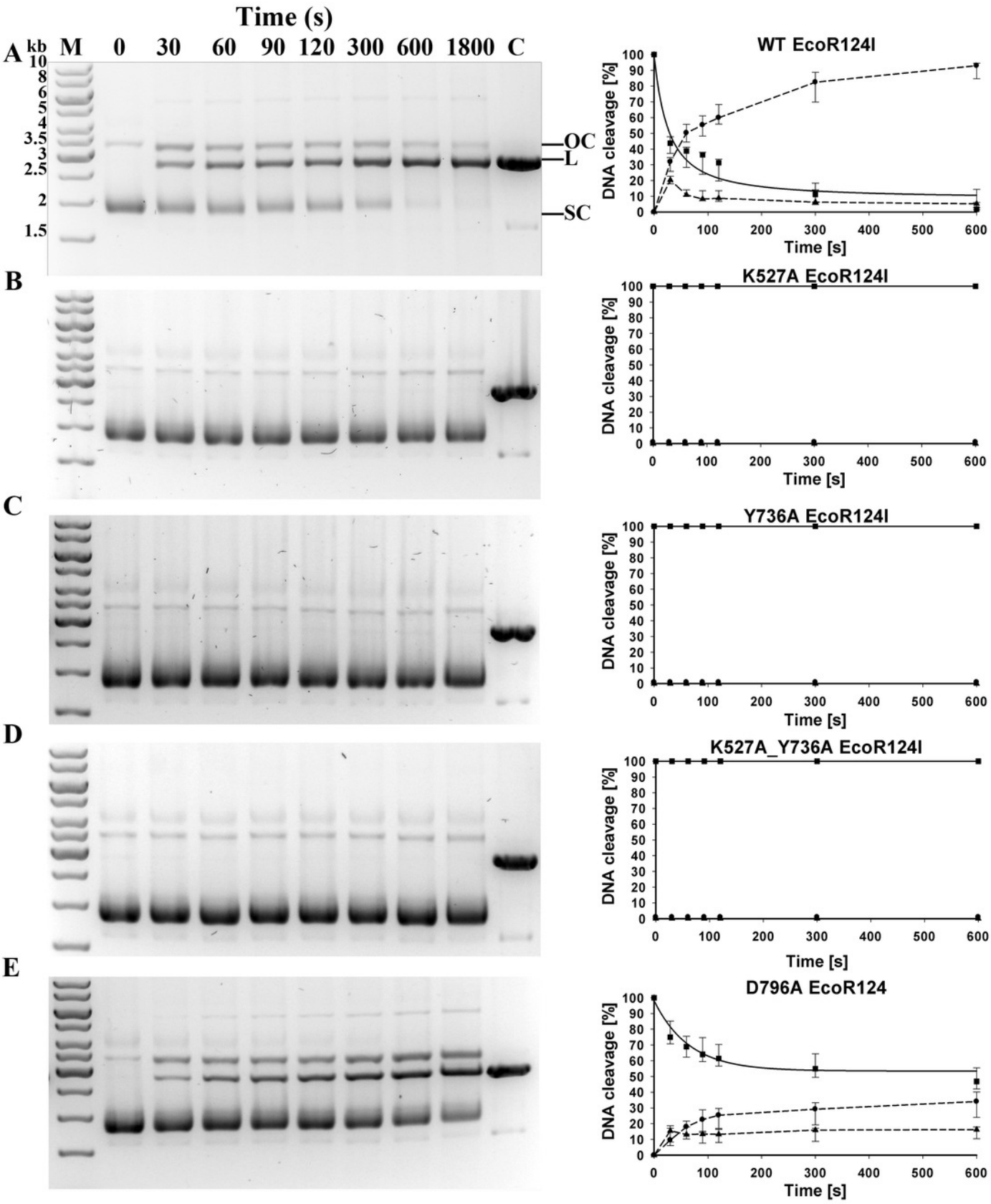
Time (s)
A
kb
M
0
30
60
90
120
300
600
1800
C
10
8
6
5
4
3.5
3
2.5
2
1.5
OC
L
SC
B
C
D
E
WT EcoR124I
K527A EcoR124I
Y736A EcoR124I
K527A_Y736A EcoR124I
D796A EcoR124
DNA cleavage [%]
Time [s]

Figure 3

Figure 3. DNA translocation analysis by triplex displacement.

Triplex-forming oligonucleotide (TFO) fluorescently labeled with TAMRA is hybridized to *linearized* DNA and translocation is initiated by addition of reconstituted enzyme and ATP as described in Methods. Fluorescence intensities after 10 min reaction time are shown. Bound (triplex) and free (displaced) TFO are indicated by lower and upper horizontal lines, respectively. From left to right, enzyme reconstituted with: wildtype HsdR, mutant K527A HsdR, mutant Y736A HsdR, double mutant K527A_Y736A HsdR, mutant D796A HsdR, unreacted triplex only, and free TFO. No triplex displacement is observed in the absence of ATP or HsdR (not shown). Average values of fluorescence intensities calculated from four or more independent experimental replicates for each individual WT or mutant enzyme species are shown.

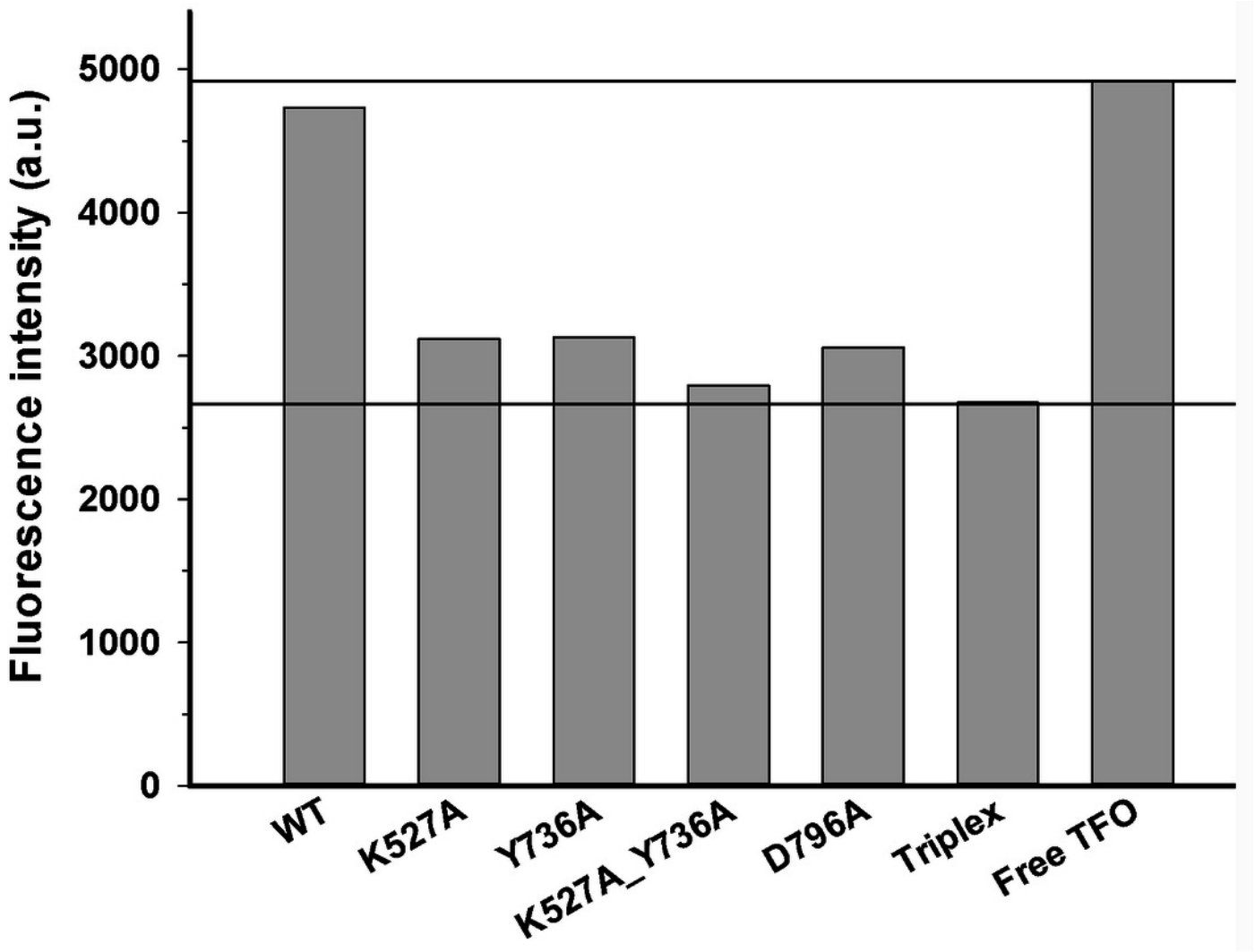
Fluorescence intensity (a.u.)
5000
4000
3000
2000
1000
0
WT
K527A
Y736A
K527A_Y736A
D796A
Triplex
Free TFO

Figure 4

Figure 4. DNA-dependent ATPase activity.

EcoR124I reconstituted from methyltransferase and HsdRs WT (black), or mutant K527A (red), Y736A (blue), D796A (green) or K527A_Y736A (dark cyan) was incubated at a final concentration of 15 nM with 90 nM circular plasmid DNA containing one recognition site and 2 mM ATP containing 0.16 µCi g-32P-ATP. At the indicated time points ATP and inorganic phosphate were resolved on cellulose TLC, autoradiographed, and scanned to quantify the extent of hydrolysis. The amount of ATP degraded is plotted as a function of time. Average values and standard deviations are calculated from at least three independent replicates for each mutant enzyme and six for WT enzyme. Data for mutants are normalized to the average value for WT at 900 sec taken as 100 %.

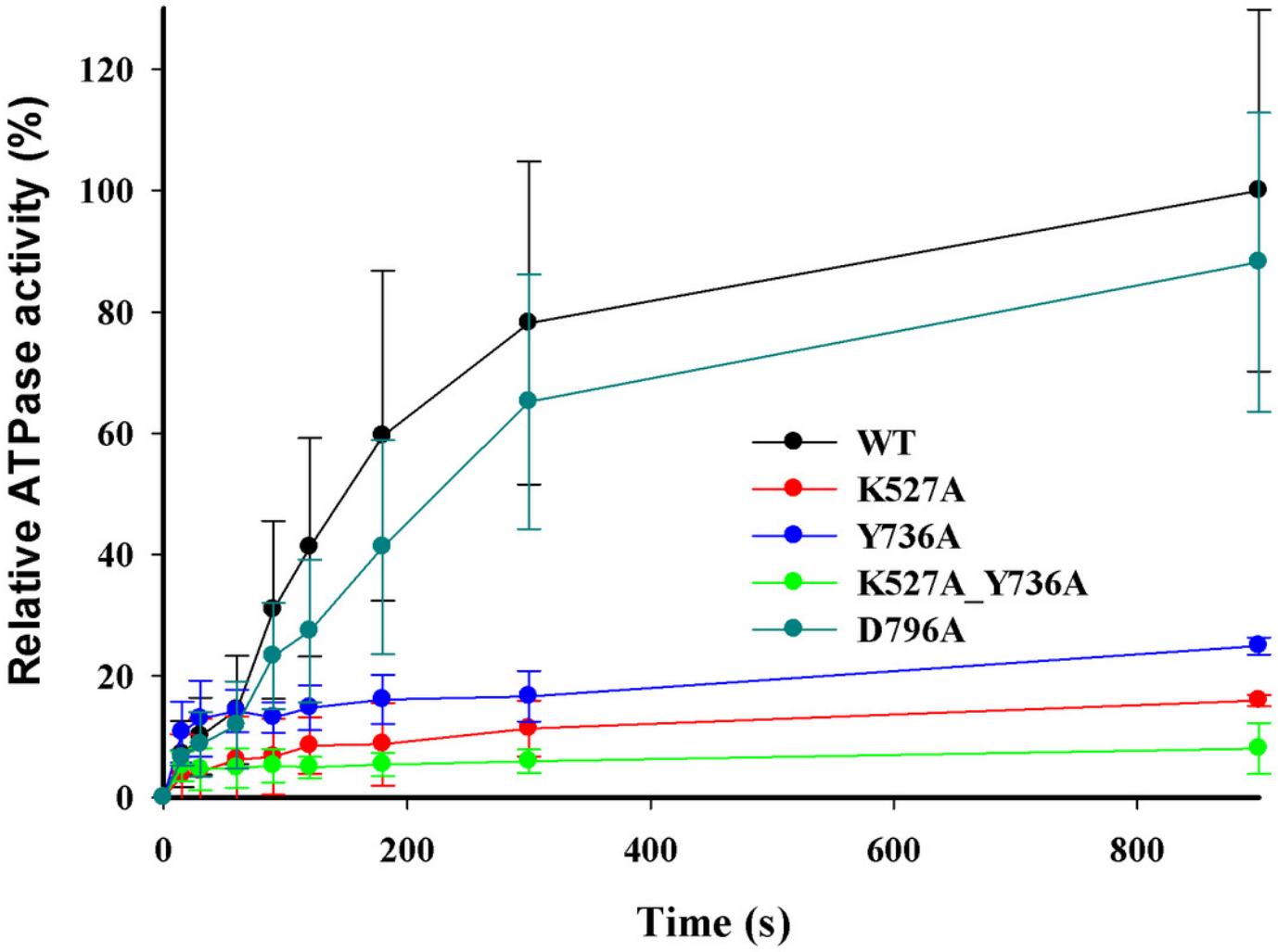
Relative ATPase activity (%)
120
100
80
60
40
20
0
0
200
400
600
800
Time (s)
WT
K527A
Y736A
K527A_Y736A
D796A

Figure 5

Figure 5. Overlay of WT and mutant structures.

Helicase domains 1 and 2 are shown in tube representation with the WT conformation in gray. Mutant conformations are overlaid on helicase domain 1, which is thus identical in all cases and therefore shown only once for better visualization. The position of each helicase 2 domain is depicted in color for each mutant (K527A, green; Y736A, blue; K527A_Y736A, red, and D796A, cyan). Mutant D796A domain 2 overlays substantially with WT, whereas the other three mutants are shifted due to the cleft opening discussed in the text.

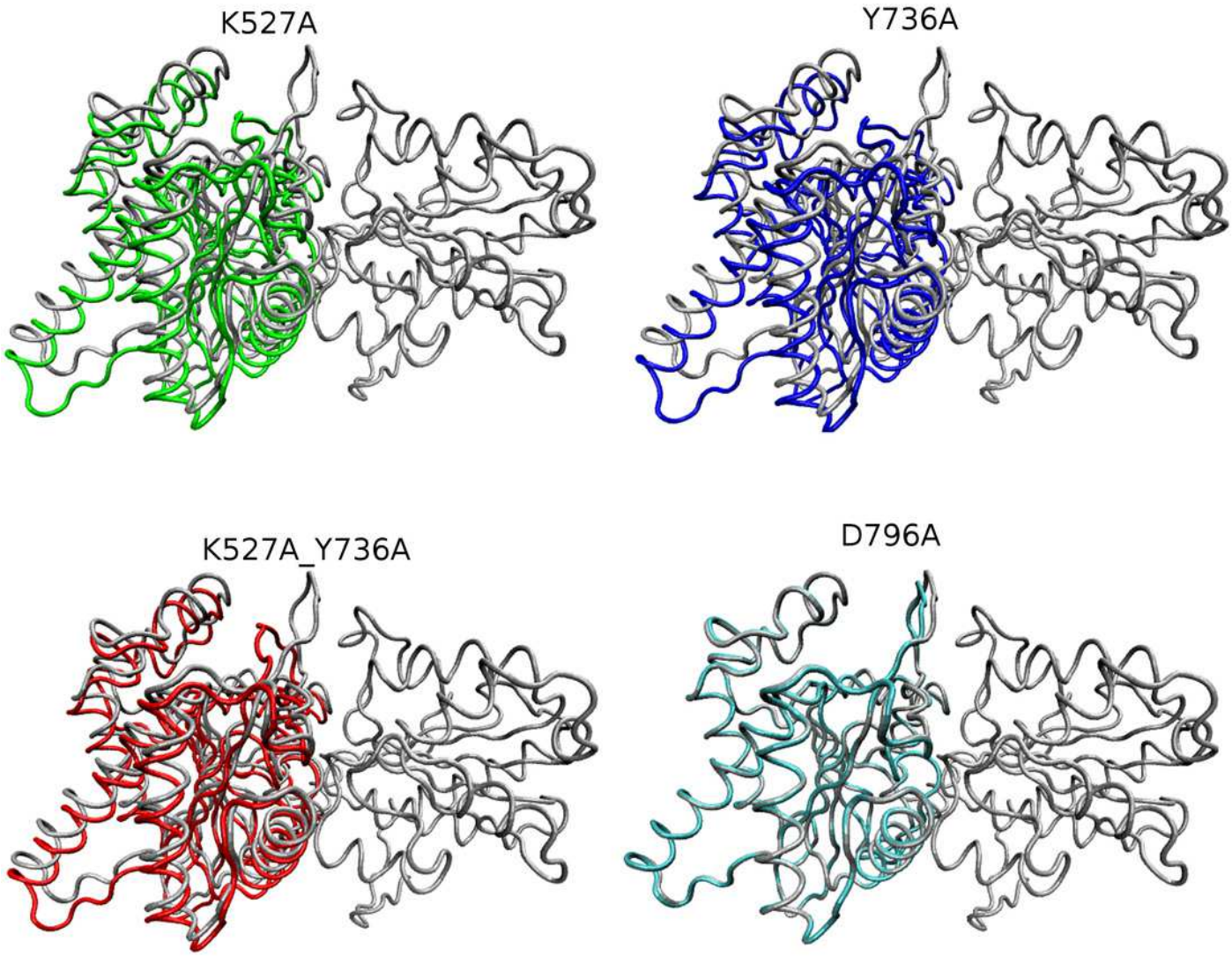

Figure 6

Figure 6. Projection of the first eigenvector of the joined trajectories in the final 20 ns of the equilibrated part of each individual simulation.

For analysis the 20 ns segments from the simulation of each protein were joined to make the composite trajectory shown. Data for the WT simulation are represented from 0 to 20 ns, for K527A from 20 to 40 ns, for Y736A from 40-60 ns, for K527A_Y736A from 60 to 80 ns, and for D796A from 80 to 100 ns.

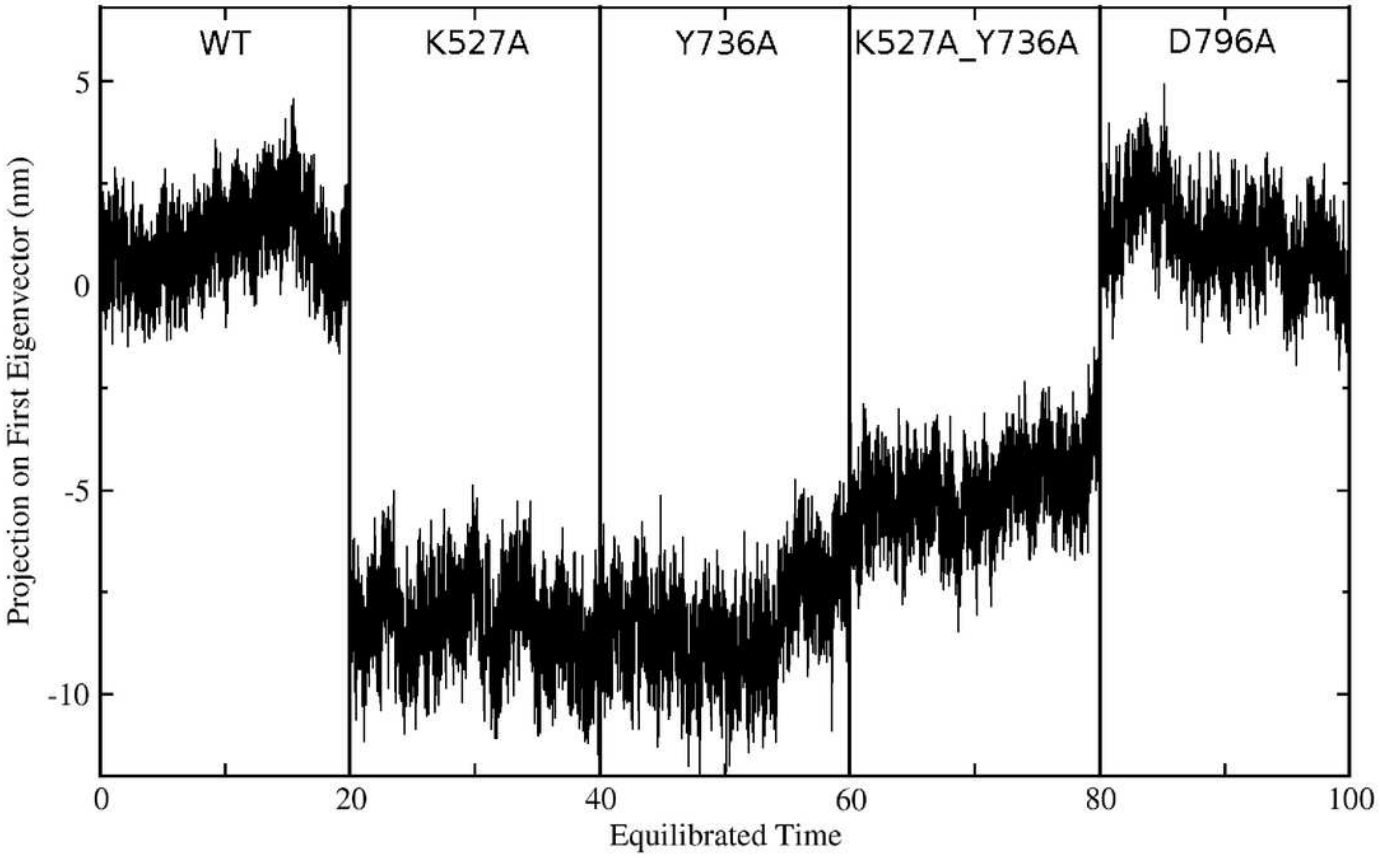

Figure 7

Figure 7. Atomic distances during the 100 ns simulations.
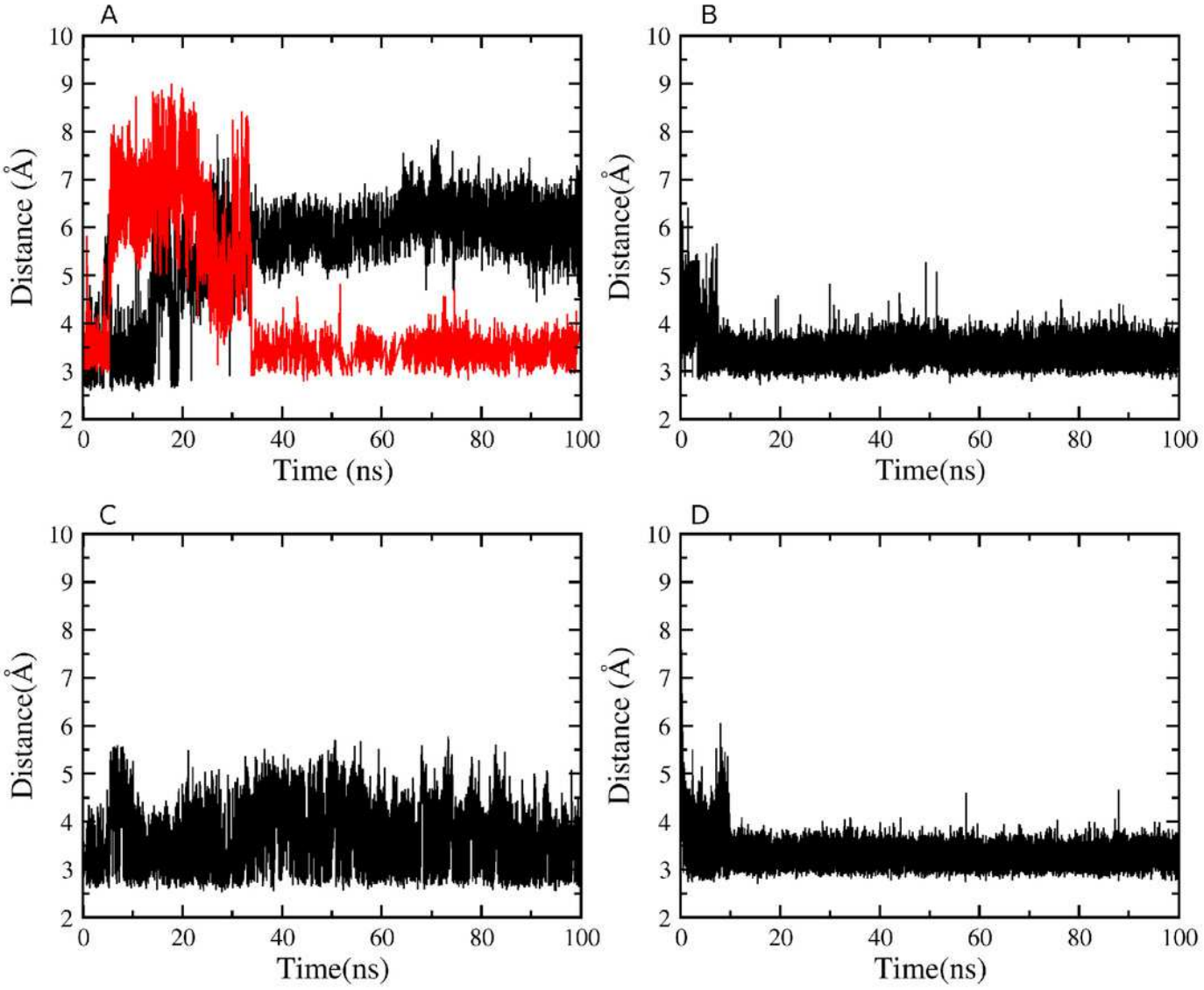
A. WT K527(Nz)-N794(O) in black, WT K527(Nz)-D796(CG) in red; **B.** WT Y736(OH)-E730(CD); **C.** mutant D796A K527(Nz)-N794(O); **D.** mutant D796A Y736(OH)-E730(CD).